# Elastic Effects of Polymer Coatings on Surface Acoustic Waves

**David L. Bartley***

*National Institute for Occupational Safety and Health, 4676 Columbia Parkway R-8, Cincinnati, Ohio 45226*

**Dawn D. Dominguez**

*U.S. Naval Research Laboratory, Code 6170, Washington, D.C. 20375*



**Surface acoustic wave (SAW) devices are presently receiving careful scrutiny for applications in chemical sensing as well as in polymer characterization. Gas monitors based on SAW sensors have the potential for miniaturization and high sensitivity to a wide variety of substances. Polymer characterization is applicable to such diverse fields as protective coating design and decontamination of polymers. To better understand the physical mechanisms behind SAW response, the effects of the elastic properties in comparison to the mass loading of polymer coatings on SAW substrates were investigated. A theoretical basis for the effects of vapor-induced swelling or of thermal expansion was established. Compressive tension and its effect on SAW frequencies were found to be simple to describe, if there is no film slippage or polymer flow. The response of quartz substrate SAW crystals coated with polycarbonate and polyimide (glassy polymers) upon exposure to toluene and methanol was measured. Practical problems as to film uniformity, thickness measurement, and environmental control necessary in such measurements are described. Contrary to recent reports in the literature, no significant elastic tightening effect was observed with these vapor/polymer pairs.**

## INTRODUCTION

Microelectronic devices are presently finding specialized applications in microsensor design—both for miniaturization and for computer–sensor hybridization. One such sensor, still in its infancy, is the surface acoustic wave (SAW) device. This device is a precise generator and detector of acoustic waves, which travel along the surface of piezoelectric crystals.

In chemical sensor applications (*1–9*), the crystal is coated with a polymer that captures the chemical of interest. Because the sorbed chemical alters the mass loading and the elastic stress of the polymer on the crystal, the SAW speed changes. Conductivity changes can also be significant (*5*) through acoustoelectric coupling but are not considered in this paper dealing exclusively with nonconductive coatings. Chemical concentrations can therefore be tracked by monitoring the wave characteristics. An array (*6, 7, 10*) of such crystals with a variety of polymers can serve as a real-time monitor or alarm, distinguishing between several gases or vapors.

An advantage of SAW devices over similar bulk-wave piezoelectric-based sensors is the potential for further miniaturization. Correspondingly, sensitivity may be increased at smaller sizes and higher frequencies because of the frequency dispersion of coated crystals. Furthermore, SAW monitoring provides an alternative approach to electrochemical sensing, should an analyte fail to produce a distinctive ionic response. Because of these advantages, SAW crystals may find future widespread use in gas monitors for measuring gas concentrations in real time.

Aside from real-time sensors, SAW devices may also be used for characterizing polymers themselves. Sorption and desorption rates determining diffusion constants are quickly measurable (*11*) because of the thinness of the films that can be used. Since equilibration times are proportional to material dimensions squared, measurements of equilibrium approach require hundredths of the time needed to characterize bulk materials.

This research was initiated as a result of the need to analyze the decontamination of polycarbonate cockpit canopies following exposure to chemical warfare agents. The central idea was that the polymer of interest could be coated on a SAW device for monitoring agent uptake and loss rates. These data could then be used to characterize the polymer/agent pair as to solubility and diffusion constants (or diffusion *functions* in the case of strongly concentration-dependent diffusion coefficients of glassy polymers). Because of the short equilibration times, a screening test would be feasible that could characterize a large number of polymer/vapor pairs quickly.

Other polymer characteristics may be measurable as well. The effect on SAWs of the drastic change in polymer elastic forces accompanying heating-induced glass transition has been reported recently in the literature (*12*). The stresses accompanying film expansion (*11*) (thermal or vapor-sorption-induced swelling, for example) may also be detectable.

Polymer characterization using SAW sensors has related applications in the field of occupational health. One possibility is to use the SAW device to characterize the effectiveness of polymers as protective coatings for equipment such as gloves or goggles. Another application is for analysis of the release of vapors back into the air from polymers that have been exposed. For example, how long would hazardous vapors be released from a fireman's coat after an exposure? A third application is, again, in the development of monitors for various hazardous gases or vapors. Polymer/vapor transfer rates are, in fact, directly relevant to monitor design in determining instrument response time as well as the reversibility and the recovery time of sensors following exposure.

Both chemical sensor design and polymer characterization require an understanding of the physical mechanisms behind SAW response, which is the aim of this paper. Specifically, the effects of the elastic properties in comparison to the mass loading of polymer coatings on SAW substrates were investigated. A mathematical analysis of such effects was developed. Finally, experiments on vapor sorption by two glassy polymers are described. Contrary to recent reports in the literature (*11*), no significant elastic tightening effect was observed with these vapor/polymer pairs.

## THEORETICAL SECTION

In this section, mathematical notation to be used is defined in describing the effect of a polymer coating on SAWs, with the substrate taken as isotropic for simplicity. The results

for the more realistic crystalline case are identical but require numerical computation for quantitative evaluation. The tensions within an expanded film are then estimated. Finally, the effect of the resulting compressive tensions on SAWs is calculated.

**Coating Effect on Surface Waves.** Distortion of an elastic body (*13–15*) may be specified by the displacement $\delta x_j$ from the point $x_j$. The displacement determines the local velocity by

$$v_j = \partial \delta x_j / \partial t \tag{1}$$

When viscous forces are negligible and at small velocities when inertial (quadratic) terms are not significant, the rate of change of the velocity $v_j$ is given in terms of the density $\rho$ and the symmetric stress tensor $\mathbf{T}_{ij}$ by the linearized form of Newton's second law:

$$\rho \, \partial v_i / \partial t = \partial \mathbf{T}_{ij} / \partial x_j \tag{2}$$

Within Hooke's approximation, $\mathbf{T}_{ij}$ is linear in the gradient of the displacement $\delta x_j$. In the case of an isotropic material, only two such tensors exist: $\Delta \delta_{ij}$ and $\mathbf{e}_{ij}$, where the "dilation" $\Delta$ is defined as the divergence of $\delta x_j$

$$\Delta \equiv \partial \delta x_j / \partial x_j \tag{3a}$$

and

$$\mathbf{e}_{ij} \equiv [\partial \delta x_i / \partial x_j + \partial \delta x_j / \partial x_i]/2 \tag{3b}$$

Therefore, the most general isotropic $\mathbf{T}_{ij}$ may be expressed by using constants $\lambda$ (Lame's modulus) and $\mu$ (the modulus of rigidity) characteristic of the material as

$$\mathbf{T}_{ij} = \lambda \Delta \delta_{ij} + 2\mu \mathbf{e}_{ij} \tag{4}$$

These equations can be applied to estimate surface wave frequencies on an isotropic solid. An uncoated material can support surface waves of frequency $\omega$ at wavenumber $k$,

$$\omega = kc \tag{5a}$$

where $c$ is the Rayleigh wave speed, determined by the cubic equation

$$(c/c_t)^6 - 8(c/c_t)^4 + 8[3 - 2(c_t/c_l)^2](c/c_t)^2 - 16[1 - (c_t/c_l)^2] = 0 \tag{5b}$$

The constants $c_t$ and $c_l$ are the transverse and longitudinal bulk-wave speeds, respectively, and are given by

$$c_t^2 = \mu/\rho \tag{6a}$$

$$c_l^2 = (\lambda + 2\mu)/\rho \tag{6b}$$

and satisfy

$$c < c_t < c_l \tag{7}$$

The surface wave frequency shift $\delta\omega_{film}$ induced by a (nonswelling) coating of thickness $d$ has been calculated (*16*) in the long-wavelength limit in the form

$$\delta\omega_{film} = dk\beta_0[-\rho'(k_t + k_l) + 4k_t\mu' c^{-2}(\lambda' + \mu')/(\lambda' + 2\mu')] \tag{8}$$

where $\beta_0$ is a constant determined solely by the substrate. Elastic constants $\lambda'$ and $\mu'$ and density $\rho'$ characterize the coating. (Primes are used in this paper generally to denote film, as distinguished from substrate, properties.) The constants $k_t$ and $k_l$ are substrate inverse penetration depths of transverse and longitudinal surface wave components, respectively, and are given by

$$k_t = k[1 - (c/c_t)^2]^{1/2} \tag{9a}$$

$$k_l = k[1 - (c/c_l)^2]^{1/2} \tag{9b}$$

Equation 8 is a consequence of the equations of motion (eq 2) together with the following boundary conditions. Suppose that the substrate occupies $z < 0$, the interface lies at $z = 0$, and the film is between $z = 0$ and $z = d$ and that surface waves move in direction $x$. Then the boundary conditions can be stated as

$\mathbf{T}_{33} = \mathbf{T}_{13} = 0$ at $z =$ $d$ (no external forces at film surface) (10a)

$\mathbf{T}_{33}$ and $\mathbf{T}_{13}$ are continuous at $z =$ 0 (Newton's third law) (10b)

$\delta x$ and $\delta z$ are continuous at $z =$ 0 (no slipping or film separation) (10c)

Equation 8 has a straightforward interpretation. Namely, the first term balances the relative densities, $\rho'$ to $\rho$, with the second term's stiffnesses. This can be seen more clearly by rearranging the equation in the following way. Although awkward algebraically, it is possible to show that eqs 5 and 9 imply that

$$1 + k_l/k_t = (2c_t/c)^2[1 - (c_t/c_l)^2] \tag{11}$$

Define a stiffness modulus $K_s$ by

$$K_s \equiv \mu(\lambda + \mu)/(\lambda + 2\mu) \tag{12}$$

Then, by using eqs 11 and 12, eq 8 can be expressed in the form

$$\delta\omega_{film} = dk^2\beta[-\rho'/\rho + K_s'/K_s] \tag{13}$$

where again $\beta$ is a positive constant dependent only on the substrate density and elastic constants. (If, as is usual, the substrate is nonisotropic, $K_s$ is dependent on the crystal plane and the orientation of the surface wave.) Equation 13 shows clearly the dependence of $\delta\omega$ on the relative densities and the stiffnesses. For example, a dense pliable film gives a negative shift, whereas a stiff low-density coating induces a positive shift. At equality between the substrate and coating properties, there is, of course, no frequency shift, but only a displacement of the wave through a distance $d$ toward positive $z$.

**Tensions in a Swollen Static Film Attached to the Substrate.** The tensions induced in an attached film (with no slippage relative to the substrate) upon swelling with dissolved vapor may be estimated by a simple mathematical construction. Other expansion mismatches between film and substrate, thermal, for example, may be handled identically. First, an unattached film is allowed to swell. Then, the swollen film is mechanically compressed along one surface to return the surface to its original, unexpanded dimensions (equivalent to reattachment to the substrate).

The tensions near the film edges are complicated. However, calculation indicates that the shear forces at the substrate/film interface oscillate anharmonically and damp exponentially to zero within roughly $d$ of the film edges. (See the Appendix and ref 17 for similar conclusions.) This means that stresses are mathematically tractable over the bulk of the film, unless edge effects are important (as in the thresholds for film slip that would therefore occur near film edges or cracks where shear forces are large). As the net force on the film is zero, the vanishing shear leaves purely constant compressive forces everywhere else within the film. In other words, except near the film edges,

$$\mathbf{T}_{11} = \mathbf{T}_{22} < 0 \tag{14}$$

and all other $\mathbf{T}_{ij} = 0$, and the displacement is constant over the film thickness. The equality of $\mathbf{T}_{11}$ and $\mathbf{T}_{22}$ means that the compression is isotropic relative to rotations about axes normal to the film in the limit of small $d$ (like a two-dimensional pressure).

The nonvanishing components of the stress tensor and the film thickness increase can be expressed in terms of an expansion coefficient $\alpha$, which is dependent on the vapor/polymer pair in the case of swelling. For concreteness, assume that the film is rectangular in $x$ and $y$ and is centered at $x = y = 0$. Suppose the unattached polymer expands according to displacements $\delta_0 x_j$ given by

$$\delta_0 x_j = \alpha \rho_v x_j \tag{15}$$

where $\rho_v$ is the vapor density within the polymer. The film is now compressed to the original dimensions in $x$ and $y$ by

$$\delta x = -\alpha \rho_v x \tag{16a}$$

and

$$\delta y = -\alpha \rho_v y \tag{16b}$$

This lateral compression induces further expansion in the $z$ direction given by

$$\delta z = \gamma \rho_v z \tag{16c}$$

where the constant $\gamma$ is determined (eqs 3 and 4) by $\mathbf{T}_{33} = 0$:

$$\mathbf{T}_{33} = [\lambda'(-2\alpha + \gamma) + 2\mu'\gamma]\rho_v \tag{17}$$

which vanishes at

$$\gamma = 2\alpha\lambda'/(\lambda' + 2\mu') \tag{18}$$

This implies that the net increase $\delta d$ in film thickness (including both the initial swelling and subsequent expansion upon lateral compression) is

$$\delta d = s'\alpha \rho_v d \tag{19}$$

where $s'$ is a constant (similar to Poisson's ratio) of the order of unity and is defined by

$$s' \equiv (2\mu' + 3\lambda')/(\lambda' + 2\mu') \tag{20}$$

Furthermore, eqs 3 and 4 imply that

$$\mathbf{T}_{11} = \mathbf{T}_{22} = -2\mu' s' \alpha \rho_v \tag{21}$$

**Effect of Compressive Film Tension on Surface Waves.** The purely lateral constant compression within a no-slip thin film swollen with solute vapor complicates boundary constraints but little—only in the geometric thickening of the film. Therefore, swelling stress has a very simple effect on surface waves moving along the film/substrate interface. Namely, the slowing of the waves by mass addition is unaffected (first term of eq 13). However, the mass effect is counteracted to a degree by a contribution from the second term of eq 13 proportional to the film thickness increase $\delta d$ calculated above. Significantly negative values of $\partial\mu'/\partial\rho_v$ or $\partial\lambda'/\partial\rho_v$, corresponding to polymer softening, decrease such counteraction.

More specifically, the only change in the boundary conditions (eqs 10a–10c) needed to accommodate film swelling is that $d$ must be replaced by $d + \delta d$ (from eq 19):

$$d \rightarrow d + \delta d \tag{22}$$

Similarly, the desired frequency shift is obtained by the same replacement in eq 13 (and within the time-dependent displacements $\delta x$ and $\delta z$). This is because the oscillatory displacements $\delta x$ and $\delta z$ are (for $z > 0$) subsequent to the compression given in eqs 16a and 16b and because stresses corresponding to consecutive displacements are additive within Hooke's linearization. Therefore, since the initial compression leaves both $\mathbf{T}_{33}$ and $\mathbf{T}_{13}$ equal to zero, stacking the displacements leaves the boundary conditions (eqs 10a–10c) satisfied.

Then, accounting for the thickness increase $\delta d$ induced by $\rho_v$, as well as polymer elasticity changes, $\partial\mu'/\partial\rho_v$ and $\partial\lambda'/\partial\rho_v$, the vapor-induced frequency shift $\delta\omega_v$ is expressed as

$$\delta\omega_v/\rho_v = dk^2\beta[-\rho^{-1} + (K_s'/K_s)s'\alpha + \partial(K_s'/K_s)/\partial\rho_v] \tag{23}$$

All of these contributions to $\delta\omega_v$ are proportional to $d$. The first term decribes the mass loading effect, whereas the second term accounts for swelling. Note that the swelling term is reduced from the mass loading term by the ratio of elastic constants in the film to those in the substrate, $K_s'/K_s$. This ratio is of the order 0.1 in the case of glassy polymers on quartz substrates. As $\alpha\rho$ is expected to be no greater than of the order of unity in the case of swelling at low vapor pressures, perhaps mass loading therefore normally dominates swelling effects in this situation. However, it is conceivable that swelling is important enough under some conditions to have an effect. The third term would account for changes in the elasticity, such as polymer softening, which would result in lowered frequency. A somewhat similar elastic constant *increase* might be observed by using SAW monitoring during polymer curing.

For describing thermal effects as reported in ref 12, $\rho_v$ is replaced by temperature shift $\delta T$ in eq 23. Also, the first term (mass loading) is omitted, resulting in only elastic effects being dominant and therefore subject to measurement using SAW monitoring. Assuming that the substrate SAW frequency is itself $T$-independent as with ST-cut quartz, the shift $\delta\omega_T$ induced by temperature change is then

$$\delta\omega_T/\delta T = dk^2\beta[(K_s'/K_s)s'\alpha_T + \partial(K_s'/K_s)/\partial T] \tag{24}$$

The constant $\alpha_T$ is a thermal expansion coefficient (differential between substrate and film).

## EXPERIMENTAL SECTION

**Film Deposition.** Polymer films of desired thickness were spun onto quartz SAW substrates by using an EC101 Photo-Resist Spinner (Headway Research, Inc., Garland, TX). Films are formed by placing a polymer solution onto the substrate, which is then spun laterally at 4000 rpm for 60 s, throwing off all but a thin boundary layer of solution that dries to form a film. Residual solvent is removed by heating. The initial solution concentration determines the film thickness. The average thickness over the substrate surface may be estimated in terms of the bulk polymer density and the measured film weight. Experiment on film reproducibility on the basis of weight indicates that a standard error equal to $\pm 0.003$ $\mu$m in the film thickness is achievable when care is taken to completely wet the substrate prior to spinning. This variability is consistent with errors expected within the weighing techniques used.

Film uniformity over the crystal is not guaranteed, however. During preliminary experiments on producing polycarbonate films, chloroform was initially used as the polymer solvent. The resulting film, shown in Figure 1, consisted of waves as tall as the polymer thickness as measured by using an interferometer. Wave-crest lines ran radially from the spin center and irregularly split into two, maintaining a roughly constant wavelength regardless of the distance from the center. This problem was solved through the use of the less volatile and more viscous chlorobenzene as the solvent.

Significant nonuniformity associated possibly with crystal edge or corner effects on the spinning/evaporation process was also observed. This can be seen in Figure 2, which indicates a strong nonlinearity in the measured film-induced SAW frequency shift vs weight-determined average (polycarbonate) film thickness (unlike eq 13). Nonuniformity, particularly near the crystal edges, is also apparent in Figure 3, showing measurements obtained by interfering light reflected from the film's surface with that from the quartz substrate, exposed by scratching the film. Clearly, a weight-averaged thickness has limited significance if the surface waves sample only the central portion of the film. Therefore, an independent, central thickness measurement must be made, or else the film thickness can be specified implicitly as the film-induced SAW frequency shift, as is now traditional in the literature.

**SAW Apparatus and Control of Noise.** Dual SAW Delay Lines (52 MHz, Part SD-52-B, Microsensor Systems, Inc., Springfield, VA) were used in these experiments. The SAW crystals used are cut along a plane that supposedly minimizes (*18*) the temperature dependence of surface wave speeds. Residual

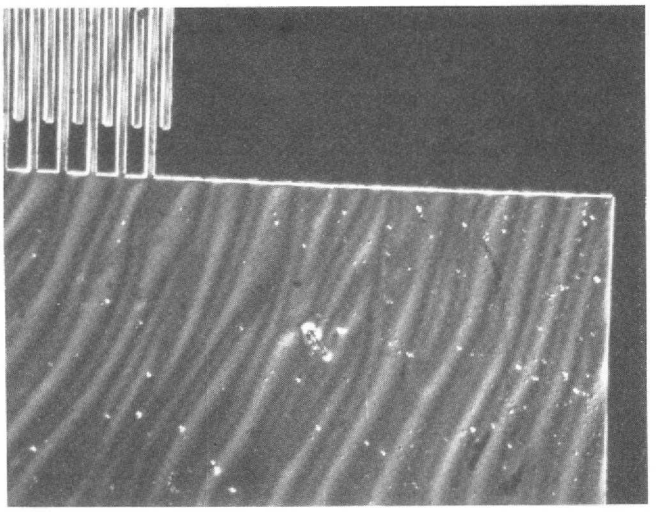

**Figure 1.** Large azimuthal waves in polycarbonate films spun from chloroform.

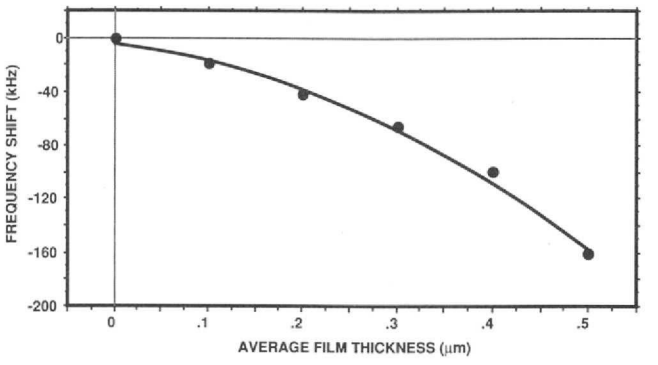


**Figure 2.** Polycarbonate film-induced SAW frequency shifts vs average film thickness as detd. by weight. The solid curve is the result of linear regression of up to quadratic terms. Standard deviation is of the order of 3 kHz.

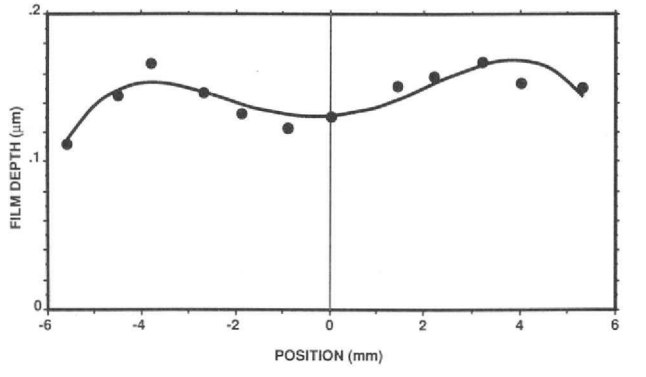


**Figure 3.** Interferometrically determined polycarbonate film uniformity.

dependency may be further reduced by utilizing *two* transmitter/receiver pairs isolated electrically and capable of sending independent acoustic waves lengthwise along the crystal surface. Each pair can separately control an oscillator whose frequency can be monitored. For use as a vapor sensor, one crystal side (containing one antenna pair) may be coated with a polymer and the other left bare. Any temperature effect equal on both crystal sides would therefore be eliminated by monitoring only the difference between the two oscillator frequencies.

Nevertheless, at a measured value of up to 700 Hz/°C, the temperature dependence was still found to be excessive for some applications. The residual temperature dependence may be caused by changes in stress at the eight electrical contacts to the SAW crystal, instead of shifts in the SAW crystal itself. Clearly, if the contacts produce a variable effect, then the nonconstancy would yet be present in the difference frequency. In any case, for

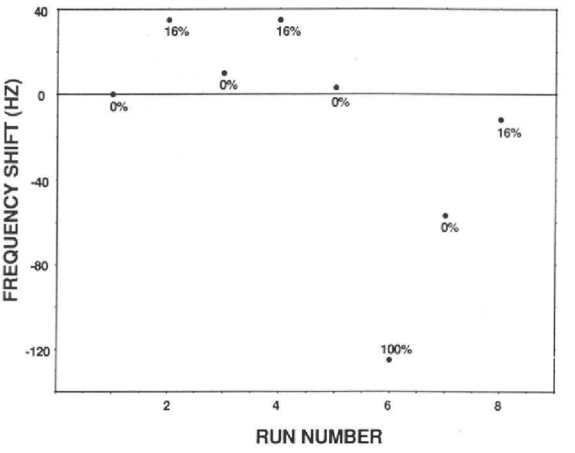


**Figure 4.** Frequency shift of the bare side of a half-coated SAW crystal at three concentrations (% saturation at 20 °C) of toluene in nitrogen. Note the lack of recovery from exposure to 100% toluene.

experiments requiring the greatest sensitivities, the entire apparatus was confined to an enclosure with the temperature controlled to 30.0 ± 0.1 °C.

Another possible problem relates to the finding that sorption on (or cross talk to) a bare quartz crystal side was found to be significant. In Figure 4 is shown the frequency shift induced on a bare crystal side, the other side being coated (with polycarbonate), by exposure to (toluene) vapor. The experiments reported here were conducted with both crystal sides coated and with only a single antenna pair monitored.

A further source of noise is traceable to the large sensitivity of the SAW device to the flow rate of gas streaming past the crystal. For example, changing the flow rate from 5 to 180 $cm^3$/min induced frequency shifts of the order of 3000 Hz. Probably this flow effect is actually a flow rate cooling effect, in other words, not independent of the temperature sensitivity mentioned above. The experiments involved switching between dilute vapor solutions and pure nitrogen ($N_2$) at a high flow rate of 180 $cm^3$/min to ensure that the dead-volume time lag was no greater than about 1 s. A constant-flow system was utilized in order to minimize flow rate cooling effects.

Finally, cooling of the vapor generation bubblers to 0 °C so as to keep vapor pressures constant may have posed a problem because of the switching between gas flows of differing temperatures. However, calculation indicated that the flow configuration used leads to nearly complete equilibration of the two lines to a single temperature prior to reaching the SAW crystal. This was confirmed by experimenting with the SAW response to pure $N_2$ cooled initially to 0 °C compared with room temperature $N_2$.

## RESULTS AND DISCUSSION

**Toluene Vapor and Polycarbonate Coatings.** The SAW response vs coating thickness and vapor concentration was measured. The vapor selected was toluene, and the coating material was polycarbonate produced by Scientific Polymer Products, Inc.—originally of interest for understanding decontamination rates from cockpit windows and safety glasses. Polycarbonate is a glassy polymer known to swell under the influence of toluene (*19*) and is therefore a reasonable candidate for the elastic effects described above.

Specifically, toluene vapor was generated at the following concentrations:

$$C = 16\%,\ 23\%,\ \text{and}\ 50\%\ \text{saturation at}\ 0\ °C \quad (25)$$

Saturated toluene at 0 °C corresponds to a toluene vapor pressure equal to 6.5 mmHg (*20*) or a concentration of about 8550 ppm. The thicknesses, as averaged over the entire crystal surface, selected were

$$d = 0.11,\ 0.21,\ 0.32,\ 0.42,\ \text{and}\ 0.58\ \mu m \quad (26)$$

These values of $d$ were measured by weighing the films as described above, assuming that the bulk density $\rho = 1.2$ g/$cm^3$

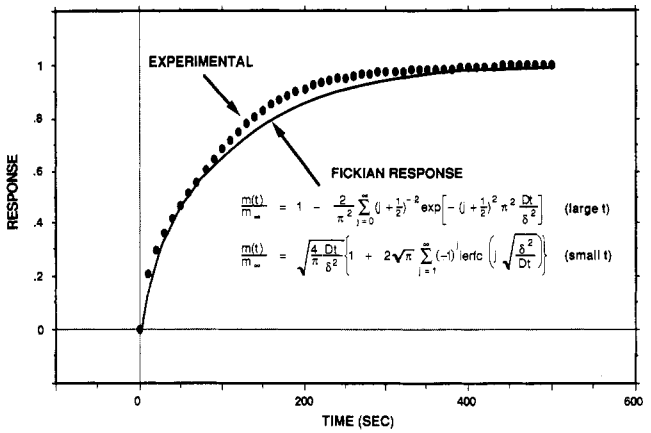


**Figure 5.** Typical response to concentration discontinuity and goodness of fit of the Fickian model.

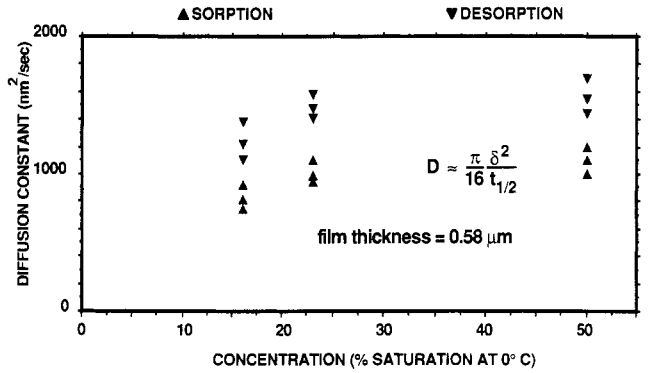


**Figure 6.** Measured diffusion constant of a 0.58-μm (by weight) polycarbonate film.

is applicable. Three sorption/desorption runs were made at each of the above values of $d$ and $C$.

A typical sorption run at $d = 0.58$ μm is shown in Figure 5. Also presented are expressions for the response according to Fick's diffusion equation (*21–24*). Two parameters are adjusted to fit the data, namely the equilibrium response and the diffusion constant $D$, which is thereby estimated. The diffusion constant is determined from the most significant term of the small-time expansion given in the figure as

$$D = (\pi/16)d^2/t_{1/2} \qquad (27)$$

where $t_{1/2}$ is the time required to reach half-equilibrium. Figure 6 shows the diffusion constant so measured at $d = 0.58$ μm. (Note that the diffusion constant is expressed here in terms of the *average* film thickness.)

The measured equilibrium frequency shifts per concentration are shown in Figure 7 with the thickness represented by the film-induced SAW frequency shfits. Important features of the data are (1) the linearity of frequency shifts vs central thickness, (2) the positive frequency shift intercept at $C = 0$, and (3) the extremely small responses at the large toluene concentrations of exposure. (Compare with the parts per billion levels reportedly detectable with some polymer/vapor pairs (*6*).)

Point 2 suggests the positive frequency shifts of film tightening. Furthermore, if the distinction between central and average film thickness were not understood, the resulting curvature observed in the sensitivity data could lead one to a conclusion that something is happening here beyond simple mass loading of the film. However, the theory presented above indicates that the dominant film-tightening effect should be $d$-proportional, rather than a positive intercept. An intercept would be more easily understood in terms of a surface adsorption (deficit) effect. Furthermore, the measured intercept is on the edge of detectability. Therefore, little can be concluded on the basis of its existence.

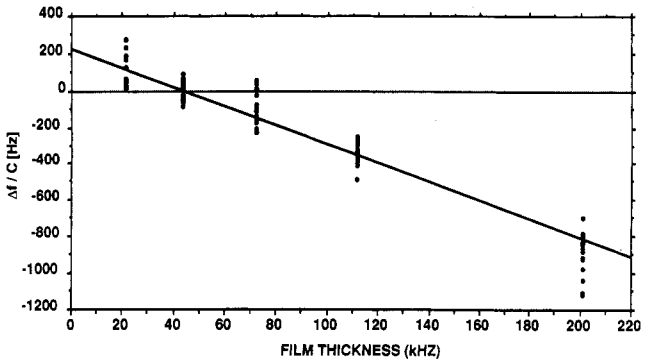


**Figure 7.** Frequency shift/$C$ (saturation fraction at 0 °C) vs film-induced frequency shift. Note linearity ($R^2 = 0.932$), which would be absent in the dependence on (weight-determined) average film thickness.

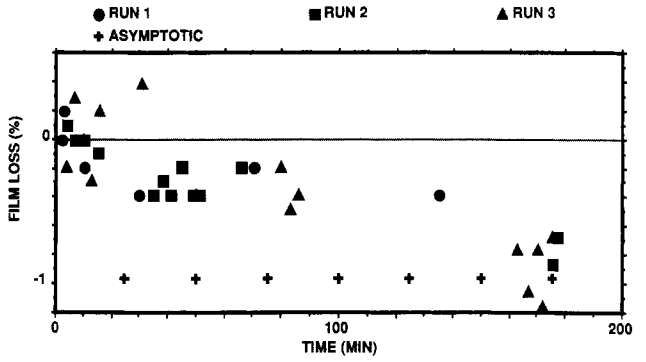


**Figure 8.** Toluene loss from a 4-μm (by weight) polycarbonate film.

Remaining is point 3. Perhaps the smallness of the measured sensitivity ($\delta f/\delta C$, which is proportional to $d$) corresponds to a cancellation between the frequency decrease from mass loading and the increase from film swelling. So as to eliminate this possibility, a separate experiment was conducted.

An independent measure of the solubility of toluene in polycarbonate was needed. To this end, a very thick film (weight-averaged thickness = 4 μm) was produced on a circular microscope coverslip by multiple spins. The use of such a thick film enabled the mass of dissolved toluene to be large enough that a crude measure of the loss during evaporation could be obtained by directly weighing the film (+ coverslip). The cost of using a thick film is in the lengthy experiments required, since the time to reach equilibrium is proportional to the film thickness squared.

In Figure 8 are the results of such an experiment entailing three all-day runs. In each case, the toluene film was exposed to 100% saturated toluene at 0 °C for 5 h to attain equilibrium (estimated by using the diffusion constants measured earlier). The film was then weighed regularly for 3 h to monitor losses.

The result is that the solubility is no greater than approximately 1% at this exposure level. Such a low solubility is consistent with the low sensitivity of the measurements described earlier. The conclusion is that there is no evidence of elastic tightening from this experiment.

**Methanol Vapor and Polyimide Coatings.** Recently, positive SAW frequency shifts have been reported (*11*) in the case of methanol solution by partially imidized polyimide (Du Pont PI-2545, E. I. du Pont de Nemours & Co., Inc., Wilmington, DE). The experiment was not designed to test for proportionality to $d$. Nevertheless, the measured frequency shift was too large to be attributed to noise. Independent verification was in order.

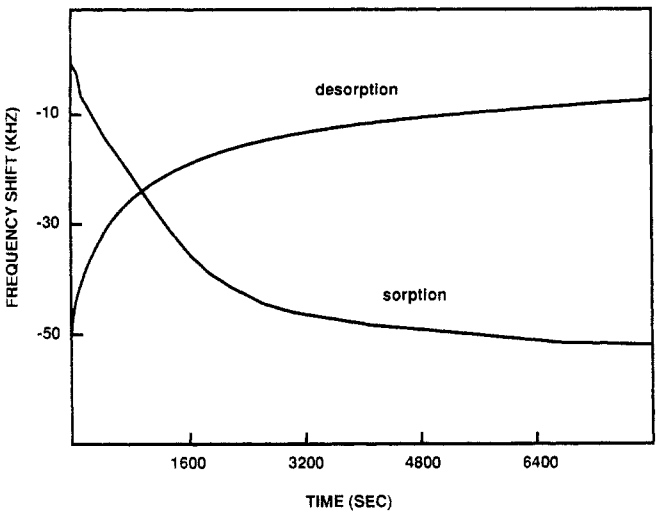


**Figure 9.** Typical sorption kinetics (note aFickian linearity) and desorption kinetics (note Fickian time dependence) for methanol in polyimide.

A (very broad) maximum (positive) shift was reported (*11*) at 25% saturation at a temperature equal to 25 °C, corresponding (*20*) to a partial pressure of approximately 35 mmHg. This is of the order of the partial pressure, 28 mmHg, of 100% saturated methanol at 0 °C. Therefore, a series of experimental runs was designed around 100% saturated methanol at 0 °C.

Two quartz crystals, A and B, were prepared with polyimide films according to procedures as identical as practical with those described in 11. The films were 3.0 $\mu$m thick by weight, assuming the bulk density $\rho$ = 1.42 g/cm$^3$. Crystal A was exposed to a discontinuous shift from pure nitrogen ($N_2$) to saturated methanol (0 °C) and, after 5000 s, return to pure nitrogen with another discontinuous shift. Crystal A was then exposed to a gradual increase in methanol concentration over 8 h as in ref 11 as a more gentle experiment, less damaging to the attachment of film to quartz. Finally, the discontinuous exposure was repeated. Crystal B received the same treatment, except that the gentle experiment was completed before the two discontinuous sorption/desorption experiments were run.

Typical sorption/desorption runs are shown in Figure 9. Note that the time dependence of the frequency shift has a linear component near the start of sorption (possibly a sign of aFickian diffusion, common in glassy polymers (*24*, *25*)). The desorption curves have aFickian $t^{1/2}$ time dependence. Correspondingly, the diffusion constants measured (with relative standard deviation (RSD) = 5%) according to eq 27 differ:

$$D_{sorb} = 0.155 \times 10^{-10}\ cm^2/s \quad (28a)$$

$$D_{desorb} = 0.255 \times 10^{-10}\ cm^2/s \quad (28b)$$

Of course, because of the linear part of the sorption curves, only the second constant has the normal meaning of a diffusion constant. Peculiarly, the diffusion constants given in eqs 28a and 28b are at least an order of magnitude less than the constants extrapolated from those reported in ref 11.

In Figure 10 are shown all the equilibrium frequency shifts for the six experimental sorption/desorption runs. The equilibrium shift magnitudes were estimated by fitting the data from the final several thousand seconds to

$$f = f_\infty + (f_0 - f_\infty)\exp(-t/\tau) \quad (29)$$

The frequency shift is clearly negative.

**General Discussion.** The purpose of this paper was to gain better theoretical and experimental understanding of

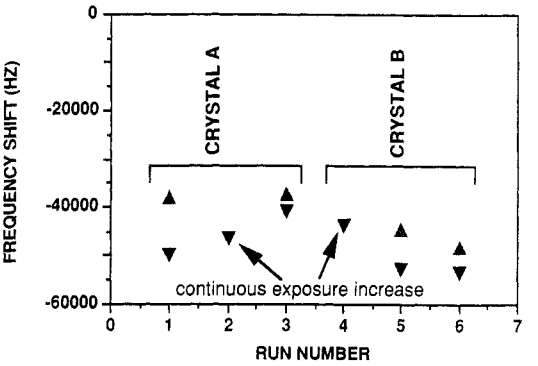


**Figure 10.** Negative frequency shifts in response of polyimide to methanol exposures. Solid and hatched symbols correspond to sorption and desorption, respectively.

elastic tightening of SAW crystal coatings. This subject is important to the application of SAW sensors in a number of aspects. The successful design of a SAW sensor depends on understanding the physics behind the workings of the device. In fact, it is conceivable that an elastic tightening effect might be purposefully designed into a practical sensor.

The successful use of SAW sensors to characterize polymers is also conditional upon understanding the response mechanism. For example, glass transitions may possibly be observed (*12*) by using SAW sensing of elastic changes in a polymer upon changing the temperature. At least three phenomena must be under control to understand the results of such an experiment: The tensions produced by the difference between thermal expansion coefficients of piezoelectric substrate and coating must be small or understood quantitatively. Expansion-induced slipping or flow of the polymer and corresponding SAW frequency drop must be absent. Other temperature effects such as those associated with the electrical contacts as described in this paper must be negligible relative to the effects to be measured.

Another area of polymer characterization concerns using SAW devices to measure the transfer of mass between a polymer and a given vapor or gas upon exposure. The extraction of diffusion coefficients from data on SAW response vs time is independent of whether elastic tightening or mass loading dominates. Aside from the asymptotic algebraic sign of the frequency shifts, the time dependence of the response is identical. However, extending the methods of ref 26 to measure solubility in glassy polymers requires quantitative understanding of tightening effects.

The experiments reported in this paper were conducted in an attempt to observe the effects of polymer coatings on SAW crystal response to vapor exposure. The largest effect of swelling would be expected to occur with glassy polymers on account of their large elastic constants and their resistance to relaxational flow relative to the substrate. However, the response of the glassy polymer, polycarbonate, to toluene was found (within the limits of experimental accuracy) to be entirely a result of simply increasing the coating mass. Similarly, the large negative SAW frequency shifts measured upon absorption of methanol by polyimide indicate at least the dominance of the effect of mass increase.

This result is consistent with the above calculation. Equation 23 indicates that elastic tightening effects should be down from those of mass loading by the ratio (about 10% with glassy polymers on quartz) of film to substrate elastic constants. Therefore, we feel that the positive shifts reported in ref 11 represent an effect not clearly understood as yet, but one other than elastic tightening or film thickening.

The experiments in this paper were limited to quartz substrates with large elastic coefficients relative to glassy polymers. More pliable substrates would accentuate the elastic

properties of the polymer coatings. Furthermore, other related sensing devices could be more strongly affected by elastic effects. For example, a sensor based on Lamb wave monitoring was recently proposed for development (27). This sensor is essentially a SAW polymer/crystal with a piezoelectric substrate so thin that the polymer coating, rather than substrate properties, dominates wave speeds. Because of the significant effect of the polymer layer, the Lamb wave sensor may be more sensitive than usual SAW sensors. Correspondingly, sensitivity to elastic changes in the polymer will be greater in this case than when the substrate more completely controls the frequency.

More information is needed regarding elastic changes in polymer coatings. Such changes can range from glass transition effects to tightening upon swelling or thermal expansion to softening upon vapor solution. Closely related data on degeneration or recovery of the polymer may be indicative of detector accuracy and reproducibility. This information can be used to draw conclusions about the practicality of SAWs and polymer coatings for gas sensors, in the ultimate design of sensors, and for SAW-monitored polymer characterization.

## ACKNOWLEDGMENT

We thank Drs. William Barger, Arthur Snow, and Hank Wohltjen for many inspiring conversations.

## NOMENCLATURE

Primed quantities refer to film properties.
$\alpha$ ($cm^3/g$), swelling coefficient
$\alpha_T$ ($°C^{-1}$), thermal expansion coefficient
$\beta$ (cm/s), positive substrate constant ($=-(k_1 + k_2)c^2\rho/(2\pi)$ in the notation of ref 1, where the substrate constants $k_1$ and $k_2 = -8.7 \times 10^{-7}$ and $-3.9 \times 10^{-7}$ $cm^2$ s/g, respectively, for ST-quartz)
$C$ (% saturation at 0 °C), vapor concentration
$c$ (cm/s), Rayleigh surface wave speed
$c_l$ (cm/s), longitudinal bulk wave speed
$c_t$ (cm/s), transverse bulk wave speed
$d$ (cm or $\mu$m), film thickness
$D$ ($cm^2$/s), diffusion coefficient
$\Delta$ (dimensionless), dilation
$\delta d$ (cm), attached film thickness increase
$\delta\omega_{film}$ (Hz), film-induced frequency shift
$\delta\omega_T$ (Hz), thermally induced frequency shift
$\delta\omega_v$ (Hz), vapor-induced frequency shift
$\delta x_j$ (cm), $j$th displacement component
$\delta_0 x_j$ (cm), displacement of free polymer
$\mathbf{e}_{ij}$ (unitless), strain tensor
$f$ (Hz), frequency
$f_\infty$ (Hz), equilibrium frequency
$f_0$ (Hz), intermediate frequency
$\phi$ (dyn), stress potential
$\lambda$ ($dyn/cm^2$), Lame's constant
$k$ ($cm^{-1}$), wavenumber
$k_l$ ($cm^{-1}$), inverse longitudinal Rayleigh component penetration depth
$k_n$ ($cm^{-1}$), $n$th complex inverse damping length
$K_s$ (unitless), stiffness coefficient (eq 12)
$k_t$ ($cm^{-1}$), inverse transverse Rayleigh component penetration depth
$\omega$ (Hz), angular frequency ($2\pi f$)
$\mu$ ($dyn/cm^2$), modulus of rigidity for isotropic material
$\rho$ ($g/cm^3$), density
$\rho_v$ ($g/cm^3$), density of sorbed vapor
$s'$ (dimensionless), elastic constant ratio of order of unity (eq 20)
$t$ (s), time
$t_{1/2}$ (s), time to reach half-equilibrium
$\mathbf{T}_{ij}$ ($dyn/cm^2$), stress tensor
$\tau$ (s), relaxation time
$v_j$ (cm/s), $j$th velocity component
$x_j$ (cm), $j$th distance component

## APPENDIX: STRESSES NEAR FILM EGES

The following is a sketch of how shear stresses vanish within a distance of the order of the film thickness $d$ from film edges. The result is the simplicity of the lateral compressive stress within the bulk of the film as described in the text. Aside from justifying hypotheses used in the paper, the details presented here may help future research into film slippage or flow, which would be most important near the film edges where the shear stresses are the largest.

Consider an infinite film extending from $x = 0$ to $x = \infty$. By superposing a linear displacement in $x$, the film with its tensions may be transformed into a system so that at $x = 0$, $\mathbf{T}_{11}$ = constant, whereas all other components vanish. The boundary conditions for $x > 0$ at the upper and lower surfaces are given by eqs 10a and 10c.

Two-dimensionality permits expression of the stress tensor in terms of a potential function $\phi$ as

$$\mathbf{T}_{11} = \partial^2\phi/\partial z^2 \tag{A1a}$$

$$\mathbf{T}_{33} = \partial^2\phi/\partial x^2 \tag{A1b}$$

$$\mathbf{T}_{13} = -\partial^2\phi/\partial x\partial z \tag{A1c}$$

The equations of static equilibrium

$$\partial\mathbf{T}_{ij}/\partial x_j = 0 \tag{A2}$$

then simplify to the diharmonic equation in terms of $\phi$:

$$\Delta\Delta\phi = 0 \tag{A3}$$

The constraints (eqs 10a and 10c) at $x > 0$ are satisfied by requiring the stress tensor potential $\phi$ to satisfy

$$\partial\phi/\partial x = 0 \quad \text{at} \quad z = d \tag{A4a}$$

$$\partial\phi/\partial z = 0 \quad \text{at} \quad z = d \tag{A4b}$$

$$-2\,\partial^2\phi/\partial x^2 + [(2\mu + \lambda)/(\mu + \lambda)]\Delta\phi = 0 \quad \text{at} \quad z = 0 \tag{A4c}$$

and

$$\partial/\partial z[(4\mu + 3\lambda)\,\partial^2\phi/\partial x^2 + (2\mu + \lambda)\,\partial^2\phi/\partial z^2] = 0 \quad \text{at} \quad z = 0 \tag{A4d}$$

(primes have been dropped for simplicity).

Because of the complexity of eqs A4c and A4d, no closed-form solution of the above equations has yet been found with $\mathbf{T}_{11}$ = constant at $x = 0$ and with the other stress components = 0. However, separation of variables provides an infinite, complete set of solutions, whose superposition can specify arbitrary $\mathbf{T}_{11}$ and $\mathbf{T}_{13}$ at $x = 0$. As described in refs 14 and 15, solutions of the biharmonic equation can be built up out of solutions of the harmonic equation, together with their products with the coordinates and specific quadratic functions containing both $x$ and $z$. The restrictive constraints (eqs A4a–A4d) over all $x > 0$ exclude factors that depend on $x$. Therefore, only functions of the following form remain:

$$\phi = \exp(-kx)\,[A\cos(kz) + Bz\cos(kz) + C\sin(kz) + Dz\sin(kz)] \tag{A5}$$

where

$$\mathrm{Re}\ k > 0 \tag{A6}$$

so that $\phi$ remains finite at large values of $x$. Substitution into the surface boundary constraints (eqs A4a–A4d) gives

$$[C + Dd]\sin(kd) + [A + Bd]\cos(kd) = 0 \tag{A4a'}$$

$$[-Ak - Bkd + D]\sin(kd) + [B + Ck + Dkd]\cos(kd) = 0 \tag{A4b'}$$

$$(2\mu + \lambda)D - (\mu + \lambda)kA = 0 \tag{A4c'}$$

and

$$\mu B - (\mu + \lambda)kC = 0 \qquad \text{(A4d')}$$

The existence of nonzero solutions implies vanishing of the determinant of the ($k$-dependent) coefficients $A$–$D$ in these four homogeneous equations, which leads to the following secular equation in terms of $kd$:

$$(3\mu + \lambda)(\mu + \lambda)\cos^2(kd) - (\mu + \lambda)^2(kd)^2 + \mu^2 = 0 \qquad \text{(A7)}$$

Numerical solution of eq A7 provides a countable infinity of solutions in the right-half complex $k$ plane for series approximation to arbitrarily specified forces at $x = 0$. The completeness of the double (Re and Im parts of $\phi$) eigenfunction set is indicated by the asymptotic

$$k_n d \rightarrow n\pi + i \ln(n\pi) \qquad \text{(A8)}$$

as can be proven for integer $n \rightarrow \infty$. Experimenting with specific values of the ratio $(\mu/\lambda)$ in eq A7 shows that the values Im $k$ are nonzero, implying oscillation in $\mathbf{T}_{ij}$ vs $x$, and that the smallest value of Re $k$ is of the order of $\pi d^{-1}$, implying quick damping in $x$.

## LITERATURE CITED


(1) Wohltjen, Hank; Dessy, R. E. *Anal. Chem.* **1979**, *51*, 1458–1475.
(2) D'Amico, A.; Palma, A.; Verona, E. *Appl. Phys. Lett.* **1982**, *41*, 300–301.
(3) Wohltjen, Hank. *Sens. Actuators* **1984**, *5*, 307.
(4) Snow, Arthur; Wohltjen, Hank. *Anal. Chem.* **1984**, *56*, 1411–1416.
(5) Ricco, A. J.; Martin, S. J.; Zipperian, T. E. *Sens. Actuators* **1985**, *8*, 319–333.
(6) Ballantine, David, Jr.; Rose, Susan L.; Grate, Jay W.; Wohltjen, Hank. *Anal. Chem.* **1986**, *58*, 3058.
(7) Wohltjen, Hank; Snow, Arthur W.; Barger, William R.; Ballantine, David S. *IEEE Trans. UFFC* **1987**, *34* (2), 172.
(8) Nieuwenhuizen, M. S.; Barendsz, A. W.; Nieukoop, E.; Vellakoop, M. J.; Venema, A. *Electron. Lett.* **1986**, *22*, 184–185.
(9) Chuang, C. T.; White, R. M.; Bernstein, J. J. *IEEE Electron Device Lett.* **1982**, *EDL-3*, 145–148.
(10) Stetter, Joseph R.; Jurs, P. C.; Rose, Susan L. *Anal. Chem.* **1986**, *58*, 860–866.
(11) Frye, Gregory C.; Martin, Stephen J.; Ricco, Antonio J. *Sens. Mater.* **1990**, *1-6*, 335–357.
(12) Ballantine, David S., Jr.; Wohltjen, Hank. *Chemical Sensors and Microinstrumentation*; ACS symposium Series 403; American Chemical Society: Washington, DC, 1989; pp 222–236.
(13) Landau, L. D.; Lifschitz, E. M. *Theory of Elasticity*; Pergamon Press: London, 1959.
(14) Timoshenko, Steven; Goodier, J. N. *Theory of Elasticity*; McGraw-Hill: New York, 1951.
(15) Leipholz, Leyden. *Theory of Elasticity*; International Publications: London, 1974.
(16) Auld, B. A. *Acoustic Fields and Waves in Solids*; Wiley-Interscience: New York, 1973; Vol. 2.
(17) Zandman, Felix; Redner, S.; Dally, J. W. *Photoelastic Coatings*; Iowa State University Press: Ames, 1977.
(18) Hauden, D.; Michel, M.; Bardeche, G.; Gagnepain, J.-J. *Appl. Phys. Lett.* **1977**, *31* (5), 315–317.
(19) Brandrup, J.; Immergut, E. H. *Polymer Handbook*; Wiley: New York, 1975.
(20) Hodgman, C. D., Ed. *Handbook of Chemistry and Physics*, 41st ed.; Chemical Rubber Publishing Co.: Cleveland, OH, 1959.
(21) Sommerfeld, Arnold. *Partial Differential Equations in Physics*; Academic Press: New York and London, 1964.
(22) Crank, J. *The Mathematics of Diffusion*; Clarendon Press: Oxford, 1975.
(23) Crank, J., Park, G. S., Eds. *Diffusion in Polymers*; Academic Press: New York, 1968.
(24) Comyn, J. *Polymer Permeability*; Elsevier Applied Science: London, 1985.
(25) Haward, R. N., Ed. *The Physics of Glassy Polymers*; Applied Science Publishers, Ltd.: London, 1973.
(26) Grate, Jay W.; Snow, Arthur; Ballantine, David S., Jr.; Wohltjen, Hank; Abraham, Michael H.; McGill, R. Andrew; Sasson, Pnina. *Anal. Chem.* **1988**, *60*, 869–875.
(27) Zellers, Edward T.; White, Richard, M.; Wenzel, Stuart W. *Sens. Actuators* **1988**, *14*, 35–45.


RECEIVED for review December 11, 1989. Accepted April 23, 1990. Mention of company names or products does not constitute endorsement by either the National Institute for Occupational Safety and Health or the U.S. Naval Research Laboratory. This work was carried out in part under U.S. Navy Contract NR677-003.

# Magnetron Rotating Direct Current Arc Using Graphite Furnace Sample Introduction for Microsolution Analysis

**David Slinkman and Richard Sacks***

*Department of Chemistry, University of Michigan, Ann Arbor, Michigan 48109*

**A direct current (dc) arc plasma in Ar or He at atmospheric pressure is formed between the tip of a W/Th wire cathode and the end of a coaxial graphite tube anode. A magnetic field parallel to the electrode axis is used to generate a motorlike rotation of the arc current channel at frequencies in the 2–3 kHz range. This results in a diffuse current sheet covering the end of the anode tube. Sample vapor from a graphite tube furnace is introduced into the arc plasma by passing the vapor through the anode tube. This ensures adequate sample–plasma interaction and results in detection limits generally in the parts per billion range. Design features of the arc–furnace system are presented along with analytical data for the elements Cu, Mn, Mg, Cr, Zn, Cd, and Fe. The results of the experiments using Ar and Ar/He mixtures as the arc plasma gas are compared.**

While the high temperatures observed in direct current (dc) arc plasmas suggest that they should be excellent excitation sources for atomic emission spectroscopy, high continuum background intensity and poor sample penetration are significant problems for solution aerosol samples. In attempts to reduce these problems, current research efforts have focused on developing dc plasma devices that entrain the sample into the hotter regions of the plasma and separate these regions from the analytical observation zone. This may be accomplished through the use of tailored gas flows and electrode positioning. A number of these plasma sources have been described in excellent reviews (*1*, *2*).

Piepmeier et al. (*3–8*) recently introduced several multielectrode dc arc devices that use either four or six electrodes to shape the plasma and efficiently entrain the aerosol sample. The six-electrode system uses three anodes and three cathodes in conjunction with quartz tubes that deliver both the Ar plasma gas and the aerosol sample. The plasma has a form similar to an inductively coupled plasma (ICP) in that the sample penetrates the center of the plasma. Since sample emission is viewed above the current-carrying portion of the plasma, the background intensity is also reduced.

0003-2700/90/0362-1656$02.50/0 